Journal of Magnetism and Magnetic Materials 469 (2019) 643–649

Contents lists available at ScienceDirect

Journal of Magnetism and Magnetic Materials

journal homepage: www.elsevier.com/locate/jmmm

Research articles

Influence of substrate effects in magnetic and transport properties of magnesium ferrite thin films

K.L. Salcedo Rodríguez[a,b,*], G. Bridoux[b,c], S.P. Heluani[c], Gustavo A. Pasquevich[a,b,d], P.D. Esquinazi[e], C.E. Rodríguez Torres[a,b]

[a] IFLP y Departamento Física, Facultad de Ciencias Exactas, Universidad Nacional de la Plata-CCT La Plata, Argentina
[b] Consejo Nacional de Investigaciones Científicas y Técnicas – CONICET, Argentina
[c] Laboratorio de Física del Sólido, Departamento de Física, Facultad de Ciencias Exactas y Tecnología, Universidad Nacional de Tucumán, Argentina
[d] Departamento de Ciencias Básicas, Facultad de Ingeniería, Universidad Nacional de La Plata, CP 1900, La Plata, Argentina
[e] Division of Superconductivity and Magnetism, Felix-Bloch Institute for Solid State Physics, University of Leipzig, D-04103 Leipzig, Germany

ARTICLE INFO

Keywords:
$MgFe_2O_4$
Thin films
Magnetism
Photoconductivity
Transport

ABSTRACT

In order to study the substrate influence in Mg ferrite properties, thin films were simultaneously grown by DC magnetron sputtering on different substrates (MgO (1 0 0) and $SrTiO_3$ (1 0 0)). In both cases samples show high values of saturation magnetization and Curie temperatures above room temperature. While in the case of the sample grown on MgO the hysteresis loops indicate the existence of more than one ferrimagnetic component and lower value of remanence to saturation ratio, the deposited one on $SrTiO_3$ is mono-component and has a rectangular-shape magnetic loop at all temperatures below 300 K. The difference is attributed to different microstructures due to the misfit strain caused by the different lattice constants between substrates and ferrite. The electric transport and photoconductivity properties have been investigated on both samples. Thin film growth on STO presents an increase around 40% of the photoconductance in the near UV range. The photocurrent shows two clear onsets that coincide with the indirect and direct band gaps of STO indicating the important role of this substrate in the generation of photo carriers.

1. Introduction

Technological advances have driven the interest and demands in the research of new materials, which show different structural, magneto-electric and magneto-optic properties with applications in the electronic industry. In this trail, transition metal oxides have received considerable attention due to its incredible variety of functional properties. From the simple binary oxides to the more complex ternary compounds, their behaviors span a wide range from insulating to semiconducting or metallic, exhibiting phenomena such as ferroelectricity, magnetism, colossal magnetoresistance or high temperature superconductivity. The extreme sensitivity of these properties to structural distortions and crystal chemistry offers many routes to controlling and engineering new functionalities. Perhaps even more stimulating is the possibility of combining the properties of individual oxides into various heterostructures, creating artificial multifunctional materials. Although such systems exploit bulk properties of the constituents, the interfaces between them play a crucial role. It is at interfaces that different properties couple, phases compete, and sometimes totally new and surprising phenomena appear such as giant magnetoresistence [1], magnetism in non-magnetic layers [2], two-dimensional electron gas [3,4].

One family of transition metal oxides that has received considerable attention are the ferrite systems with spinel structure. Due to nanoscale effects and the high cation distribution dependency to the synthesis process, ferrites system found a wide range of applications: magnetic storage and imaging devices, magnetic sensors, high density storage devices [[5] and references there in], magnetic assisted drug delivery, magnetic hyperthermia treatment [6], pigments [7], environmental remediation [8] etc. Also, there are important modifications in ferrite nanosystems due to interface influences and strain induced during fabrication. For example, is it possible obtained more stable magnetic systems [9,10], samples with enhanced photoluminiscence [11,12], good electrochemical activity [13], etc. As is well known, MFe_2O_4 (M: transition metal) spinel structures present two kinds of oxygen coordination sites: tetrahedral sites, where the ion is surrounded by four oxygen atoms (A-Sites) and the octahedral sites, where the ion is surrounded by six oxygen atoms (B-Sites). Depending of the number of Fe

* Corresponding author at: IFLP y Departamento Física, Facultad de Ciencias Exactas, Universidad Nacional de la Plata-CCT La Plata, Argentina.
E-mail address: klsalcedor@fisica.unlp.edu.ar (K.L. Salcedo Rodríguez).

https://doi.org/10.1016/j.jmmm.2018.08.065
Received 26 February 2018; Received in revised form 23 August 2018; Accepted 23 August 2018
Available online 08 September 2018
0304-8853/

ion in A sites (Fe_A), this system can be normal spinel ($Fe_A = 0$), mixed spinel ($0<Fe_A<1$) or inverted spinel ($Fe_A = 1$). In particular, magnesium ferrite $MgFe_2O_4$ (MgFO), with a mixed spinel structure ($\sim Fe_A = 0.1$), is a promising candidate for spintronic applications due to it is a soft ferrimagnetic n-type semiconductor with a high Curie temperature ($T_C \sim$ 710 K). Other important aspects are its high sensitivity to humidity [14], chemical stability and a band gap of 2.0 eV, making it a promising candidate for a wide range of applications in, e.g., heterogeneous catalysis [15], sensors [16], organic contaminants [17], lithium ion batteries [18], photo-electrochemical water splitting method [19].

Although epitaxial MgFO thin films (TF) are of great interest from both fundamental and practical perspectives, relatively little attention has been paid to the study of these systems. Some studies of epitaxial MgFO films growth on STO [20], sapphire [21] and MgO [22] by pulsed laser deposition, and molecular beam epitaxy were reported in literature. In all cases ferrimagnetic TF, whith saturation magnetization between 115 and 195 emu/cm^3, coercitivities between 200 and 700 Oe and high magnetic anisotropy were obtained. In the case of MgFO deposited on STO [20] TFs present negative magnetoresistance attributed to the presence of anti-phase boundaries. In these published articles, authors study how magnetic and/or transport properties are influenced by the fabrication conditions mainly, oxygen pressure, TF thickness and post annealing treatment. However, there are no reports of the influence of the interface with substrate in this kind of systems.

In this work, we present a study of MgFO thin films that were growth simultaneously in two different substrates: $SrTiO_3$ (STO) and MgO, in order to study the influence of these interfaces in its structural, magnetic and transport properties. The topography, cation distribution, magnetic response with applied field and temperature and transport and photoconductivity behavior were studied. In all cases transparent, ferrimagnetic (with high T_C) and semiconductor thin films were obtained. The sample grown on STO presents a highly square magnetic loop, an important photoconductivity response and strong evidences that conduction is partially through the STO substrate.

2. Experimental details

The magnesium ferrite thin films were deposited on two different substrates, (1 0 0) MgO and (1 0 0) STO (MgFO-MgO and MgFO-STO) simultaneously, by DC sputtering using Fe and Mg metallic targets under oxygen atmosphere. The samples consist of 5 bilayers of 6 nm Fe-O and 2.2 nm Mg-O films each, with a total thickness of approximately 41 nm. The multilayer films were grown starting with a base pressure of 2×10^{-7} mTorr and an operation pressure of 15 mTorr under Ar and O gas flow at 24 ml/min and 1 ml/min, respectively. The supplied DC power was 200 Watts. The deposition was carried out at a substrate temperature of 973 K in order to favour the interlayer diffusion. Deposition rates were 0.07 Å/s and 0.65 Å/s for Fe-O and Mg-O monolayers, respectively. To compare the structural and magnetic properties of the films with those of a bulk system, a bulk $MgFe_2O_4$ sample was synthesized using a ceramic method, i.e. MgO and Fe_2O_3 powders were mixed in a ratio 1: 1 using an agate mortar and pressed and calcinated at 1000 ^{O}C during 10 h in air.

The films were structurally characterized using X-ray Diffraction (XRD). XRD patterns were recorded by $\theta-2\theta$ scans with CuKα radiation ($\lambda = 0.15406$ nm). Topographical features of the thin films were analysed by Atomic Force Microscopy images using a NT-MDT SMENA Solver-PRO configured in tapping mode. The elemental analysis was performed by Energy Dispersive X ray Spectroscopy (EDX). The measurements were carried out at 20 kV acceleration voltage using a Quanta SEM FEI Microscope, equipped with EDX. X-ray absorption spectroscopy (XAS) measurements at K and $L_{2,3}$- Fe and Ti edges and X ray magnetic circular dichroism (XMCD) at $L_{2,3}$-Fe edge were performed in the beamlines of the Brazilian Synchrotron Light Laboratory-LNLS (Campinas, Brazil). Fe and Ti K-edge XAS measurements were performed at XAFS2 beam line in transmission mode. Fe $L_{2,3}$ XAS and XMCD measurements were realized in the Planar Grating Monochromator (PGM) beamlines. XMCD measurements were carried out using circularly polarized light and applied magnetic field between ± 0.6 T. The absorption data were collected in the Total Electron Yield (TEY) mode. More details about the general protocol used in the XMCD measurement see [23,24]. Both, XAS and XMCD measurements were performed at room temperature. In order to analyse these results, we also performed XAS measurements to Fe oxides references powders as FeO, Fe_3O_4 and $\alpha-Fe_2O_3$.

The magnetic properties were studied using a Quantum Design MPMS superconducting quantum interference device (SQUID) magnetometer. Magnetization field hysteresis loops were obtained at 5 K, 10 K, 100 K and 300 K and temperature hysteresis by Zero Field Cooling and Field Cooling curves (ZFC-FC) with an applied field of 50 Oe. Also, vibrating sample magnetometer measurements (VSM) was performed at room temperature with a maximum field of 2 T, which was applied on perpendicular and parallel directions.

The electrical resistance at room temperature was measured with electrodes prepared by clenching gold wires with indium on the films. Electric transport and photoconductivity spectroscopy measurements (PCS) were performed in a closed-circuit system of helium (temperature range 10 K–340 K up to 0.8 T). A xenon 1000 W lamp was used for excitation and an Oriel monochromator. The wavelength sweep rate used for the measurements of photoconductance spectra was 0.5 nm/s.

3. Results and discussions

3.0.1. XRD, AFM and XANES characterization

Fig. 1(a) shows the XRD pattern of MgFO-STO. The $MgFe_2O_4$ (4 0 0) reflection is observed in addition to the STO ones, indicating an epitaxial growth of MgFO on (0 0 1) STO substrate without any additional phase. However, the unit cell parameter obtained for MgFO-STO is a= 8, 433 Å(perpendicular direction), which is higher than reported for bulk $MgFe_2O_4$ by Sheikh Manjura Hoque [25]. In MgFO-MgO sample case, see Fig. 1(b), because the MgFO (4 0 0) reflection is near to the substrate (2 0 0) reflexion, due to similar unit cell parameter, a shoulder can be distinguished, which is not observed in the MgO substrate (indicated by the arrow in the figure), confirming the epitaxial grown of MgFO on MgO substrate at (0 0 1) direction, too. The obtained stoichiometry ratio by EDX was Fe/Mg ≈ 3 for the MgFO-STO sample. Taking into account that both samples were grew simultaneously, we assume that the Fe/Mg ratio is similar for the two samples. This ratio indicates that the samples are not stoichiometric. Nevertheless, the Fe ions appear to be not segregated in other crystallographic phases but spinel structure is conserved.

Fig. 2 shows the AFM 3D images and the transversal profile for both films within an area of 100 μm^2. The 3D images (Fig. 2)) and transversal profiles (Fig. 2(b) and (d)) indicate a clear difference in the morphology between the two thin films. The morphology of MgFO-STO film (Fig. 2(a)) has a columnar formation (~ 20 nm height) with a root-mean-square (RMS) surface roughness of 2.37 nm. In contrast, the RMS= 0.43 nm obtained for the MgFO-MgO is smaller indicating a smoother superficial texture (Fig. 2(d)). Both samples present a grain size around 100 nm. Taking account the difference between MgFO lattice parameter (a = 8.367 Å [25]) and STO and MgO ones (2a= 7.80 Å and 2a= 8.42 Å) there is a structural mismatch of −6.7% between the unit cell of MgFO and a double unit cell of STO substrate and a smaller than 1% in the case of MgO substrate. The mismatch difference between the two substrates and the film in the interface zone could generated the difference of the growing mechanics, defining the surface features. MgFO-MgO sample grown on MgO substrate, which has a cubic structure as the Mg ferrite, and a cell parameter more similar to the thin film, present a lower roughness. In contrast, MgFO-STO sample, grown on a substrate with perovskite structure ($SrTiO_3$), presents a major roughness. The increase in roughness could be a

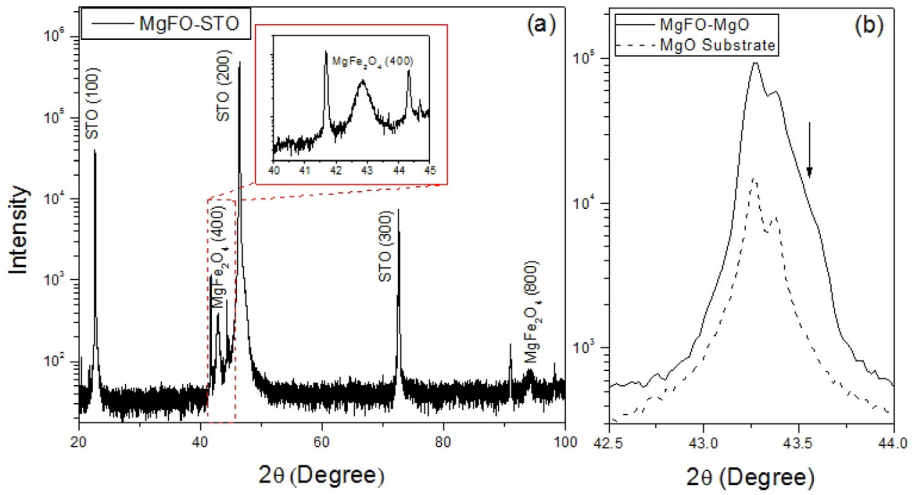

Fig. 1. XRD patterns of (a) MgFO-STO thin film in a region $20 < 2\theta < 100$ degrees. The MgFO peaks appear at low and high angles. Peaks of the substrates are recognized too. (b) Similar for the MgFO-MgO thin film in the region $42.5 < 2\theta < 44$ degrees. In this case the peak due to the MgFO is recognized as a shoulder, which is not observed in the substrate alone (dashed line).

consequence of the major strain present in this sample in the interface MgFO-film/STO substrate during the growing, modelling the surface.

Fig. 3(a) and (b) present the XANES measurements at the Fe-K edge for both samples. The results are in good agreement with the spectrum of bulk MgFO, indicating that Fe ions environment is similar to the expected for Mg ferrite. However, a small shift to lower energies at the absorption edge was identified for both samples. This shift suggests a mixed oxidation state of the Fe atoms, which is expected due to the Fe enrichment observed in the EDS measurements. In order to confirm this assumption we show a fit obtained from a linear combination of $MgFe_2O_4$ and Fe_3O_4, see Fig. 3(c) and (d), assuming 28 at.% and 22 at.% of magnetite in MgFO-STO and MgFO-MgO, respectively. This result implies that there is a 14 at.% (11 at.%) of ions with 2+ oxidation state and not necessarily the segregation of magnetite. It is important to clarify that samples do not have magnetite. There is no evidence for any secondary phase other than Mg ferrite. Magnetite spectrum was used to determine the fraction of Fe^{2+} because in magnetite (i.e. an inverted ferrite) the local environment of Fe^{2+} and Fe^{3+} is similar to Mg ferrite. Therefore, we expect that their contribution to XANES is similar. If the samples would have such an amount of segregated magnetite, we should have seen in the XRD spectra.

3.1. Magnetization and XMCD results

The FC magnetization curves (not shown) are nearly temperature independent between 5 K and 300 K, suggesting Curie temperatures

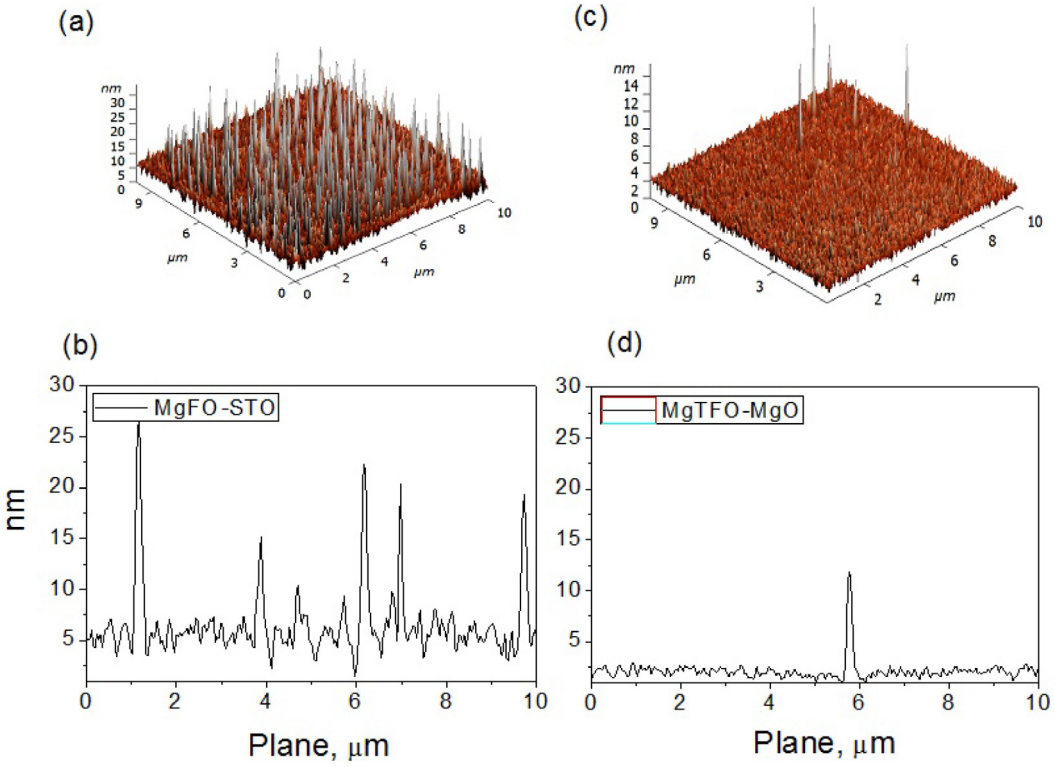

Fig. 2. Surface 3D AFM images of the MgFO thin films grown on (a) STO and (c) MgO substrates and a transversal profile for (b) MgFO-STO and (d) MgFO-MgO.

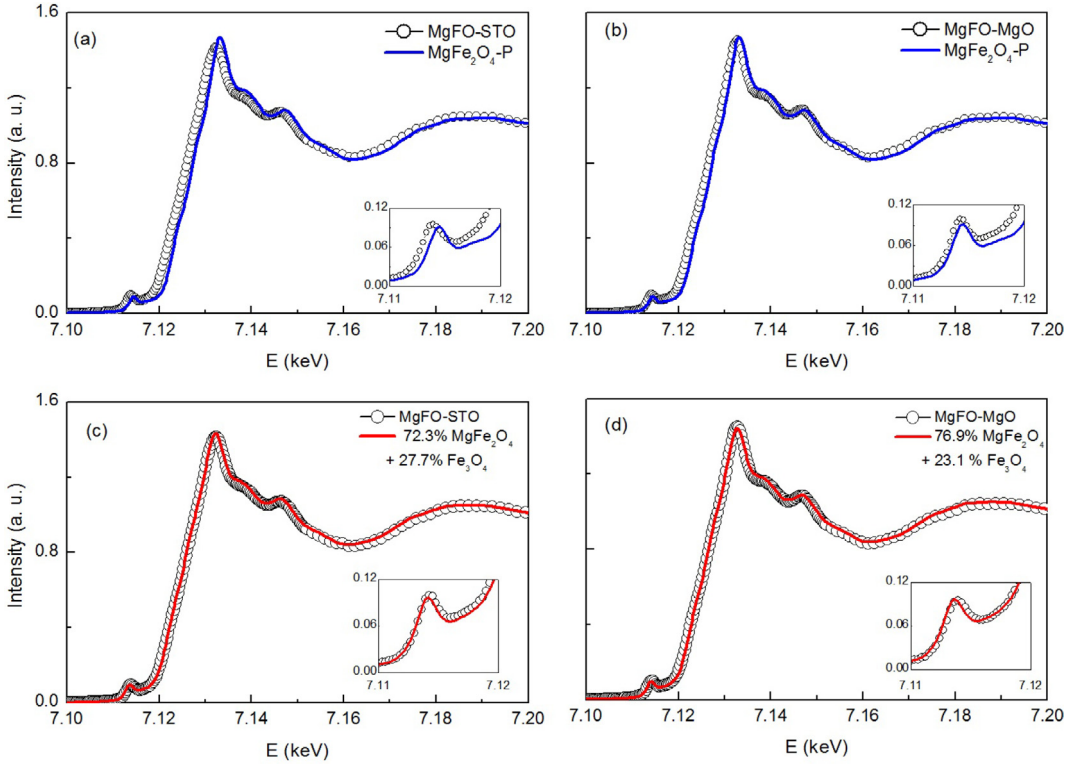

Fig. 3. XANES spectra at the Fe-K edge of (a) MgFO-STO and (b) MgFO-MgO samples. The continue lines show the results obtained for the bulk $MgFe_2O_4$ reference sample ($MgFe_2O_4$-P). (c and d) Spectra of the thin films compared with the ones resulting from a linear combination of Fe_3O_4 and the $MgFe_2O_4$-P experimental spectrum. The insets show the pre-peak regions.

higher than room temperature for both samples. The ZFC and FC curves measured at 50 Oe applied parallel to the main surface of the films show small differences indicating that domain wall pinning and/or magnetic anisotropy may play a role.

Fig. 4 (a) and (b) shows the hysteresis loops for the two samples. The MgFO-STO sample shows a rectangular hysteresis loops at all temperatures with high remanence (M_r) to saturation magnetization (M_s) ratio $M_r/M_s \sim 0.8$. From the field derivative of the decreasing field part branch of the cycle (Fig. 4 (c)) we conclude that there is a unique ferrimagnetic component with a coercive field that decreases with

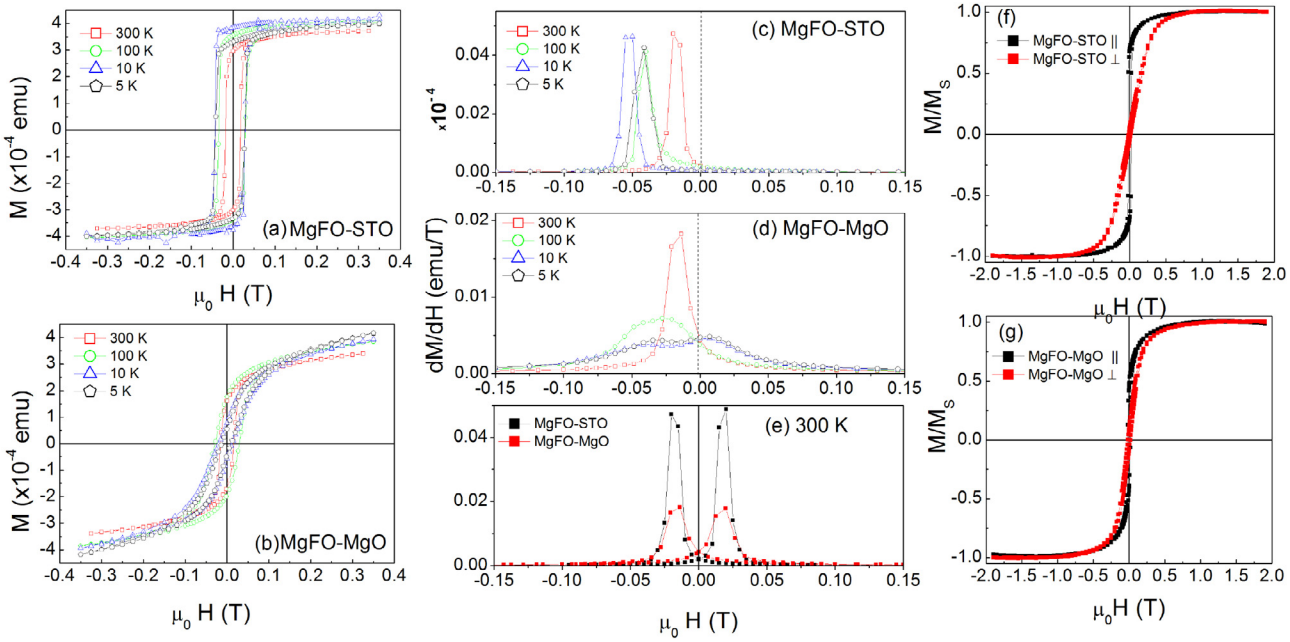

Fig. 4. Hysteresis cycles of MgFO-STO (a) and MgFO-MgO (b) taken at 5, 10, 100 and 300 K with a maximum applied field of 0.35 T parallel to the main surface. First derivative of the magnetization hysteresis loops for MgFO-STO (c) and MgFO-MgO (d) and comparison between both samples at 300 K (e). Hysteresis loops measured at room temperature with applied field parallel and perpendicular to the plane of the samples for MgFO-STO (f) and MgFO-MgO (g), the curves were registered between −2 and 2 T, but it is shown a reduce range for clarity.

temperature between 10 and 300 K(with a maximum H_c(10 K) = 0.053 T) and at 5 K the coercivity decreases.

In contrast, the hysteresis cycles of the MgFO-MgO sample (Fig. 4(b)) show a smaller M_r/M_s ratio and from the derivative (Fig. 4 (d)) we infer the presence of more than one magnetic component in measurements below 300 K based on the two different coercivities observed. One of the components has null coercivity and is clearly distinguish from the other in the 5 and 10 K measurements. This component confire the S-shape characteristic of the M-H loops. It is usual, the observation of this behavior in nanometric ferrite systems [26] and it has been assigned to surface spin canting effect [10]. The other component has coercivities in the order of the unique component of MgFO-STO sample. At room temperature, M_s of both samples are similar (MgFO-STO: 364 emu/cm^3 and MgFO-MgO: 330 emu/cm^3) and also the coercivities (H_c = 0.02 T and H_c = 0.017 T, respectively) as can be obtained from the derivatives (Fig. 4(e)). The obtained saturation magnetization is higher by 70% approximately, than the previously reported for similar systems [27,20,28].

The main difference between both samples is the shape of the magnetic hysteresis loops. The conditions to obtain a rectangular loop (as in MgO-STO thin film) for a ferro or ferrimagnetic material can be [29]: (i) high degree of symmetry and several axes of easy magnetization, (ii) high crystallographic anisotropy, (iii) magnetic coupling between grains (iv) homogeneity of grain size and/or (v) microscopic inhomogeneities which acts as anchors of the walls of domains. The condition (i) is common in cubic structures as ferrites with spinel structure. In order to confirm condition (ii) we performed measurements with the applied field parallel and perpendicular to the sample plane (see Fig. 4(f) and (g)). It can be seen that the film grown on STO shows a higher magnetic anisotropy, which could be considered a consequence of unit cell parameter distortion (contraction in the plane, compensated for a lengthening in perpendicular plane direction as was mentioned in Section 3.0.1) generated by the epitaxial growing. The enhancement of anisotropy energy helps in holding the magnetic moments in a certain direction by prevent spin canting. This effect has been observed in other ferrite systems [9].

The uniformity of grain size were confirm in both samples by AFM measurements and concerning the microscopic inhomogeneities the main difference between both samples are the superficial columnar formations observed in the MgFO-STO sample (see Section 3.0.1). The last is probably the main reason that induces the high value of M_r/M_s ratio. Because the geometry of both samples was the same, the observed differences are not related to a shape anisotropy.

Fig. 5(a) shows the XAS $L_{2,3}$-Fe spectra for the MgFO-STO sample, carried out with applied fields ± 0.6 T. The corresponding XMCD signal is shown in Fig. 5(b). The L_3-Fe XMCD signal presents one positive and two negatives peaks. The positive peaks correspond to Fe^{3+} ions in A sites and the negative ones to Fe^{3+} in B sites [30]. The negative peak corresponding to Fe^{2+} in XMCD spectrum of MgFO-STO sample, overlap with the first negative peak of the Fe^{3+} one and only modify its relative intensity as can be seen for the case of magnetite in Fig. 2 of Ref. [31]. Iron ions in A sites are aligned antiparallel and those in B sites that are parallel to the applied field. From the relative intensities of the A and B peaks I_B/I_A, it is possible to determine their relative occupation $X_B/X_A \sim 1.5$ in A and B sites [31].

Taking account the concentration Fe/Mg~ 3 determined by EDX and $X_B/X_A \sim 1.5$ from XMCD, it is possible to obtain the compositional formula for the Mg ferrite thin film as $(Fe^{3+}_{0.9}Mg_{0.1})_A[Fe^{3+}_{1.14}Fe^{2+}_{0.21}Mg_{0.65}]_BO_4$. Then, the Mg ions occupy only 10 % of the A sites, as previously reported for stoichiometric Mg ferrites [32]. The Fe ions in this ferrite occupy B sites with 2+ (7%) and 3+ (93%) oxidation. The percentages of 2+ and 3+ oxidation states are deduced from the percentage of the magnetite-like contribution obtained from the XANES fit (28%).

This explains the high value of saturation magnetization observed: there is ferromagnetic coupling between Fe_B sites not only due to the inversion, which is the usual mechanism in Mg ferrites, but also due to the double exchange interaction between Fe^{2+} and Fe^{3+} ions in B sites.

3.2. Transport measurements

Fig. 6 shows the temperature dependence of the resistivity of the two samples. The behaviour is the typical one for semiconducting materials. The resistivity of the samples obtained from their resistance and geometry is $\rho(300K)_{MgFO-STO} = 24.0$ Ω mm and $\rho(300K)_{MgFO-MgO} = 4.0$ Ω mm. The difference in absolute values of the resistivity and in the temperature dependence between the two samples can be simply due to the parallel contribution of the less resistive interface between MgFO and STO. It was previously reported that STO substrate can reduce during the fabrication of the film [33]. The oxygen vacancies at the interface substrate/film induce a n-type semiconducting character lowering the resistivity with respect to the bulk.

As can be seen in Fig. 7(a), the electrical resistivity of both samples show a non-Arrhenius temperature dependence. Only at high temperatures, between 160 K and 300 K (see inset in Fig. 7(a)) the samples appear to follow an Arrhenius behavior. From the linear fits to $\ln(\rho/\rho_0)$ vs. $1/T$ the values obtained for the apparent activation energy are E_a = 99.25 ± 0.04 meV and 82.17 ± 0.02 meV for MgFO-MgO and MgFO-STO, respectively. At lower temperatures a hopping transport mechanism comes into play, in which the carrier transport does not longer take place via band states but instead by tunnelling hopping between localized states, as the variable-range hopping (VRH) mechanism. The temperature dependence of the resistivity in the VRH can be represented as $\rho = \rho_0 exp(T^*/T)^{\beta}$ [30,31] where ρ_0 is constant and T^* is a material dependent characteristic temperature, proportional to the inverse of the density of states at the Fermi level and a localization length.

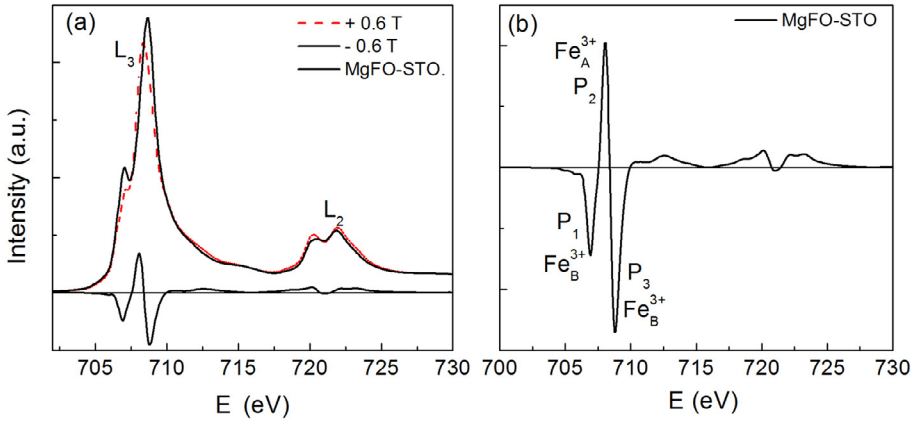

Fig. 5. $L_{2,3}$-Fe edges XAS spectra of the MgFO-STO sample with an applied field of 0.6 T. (b) XMCD signals for MgFO-STO.

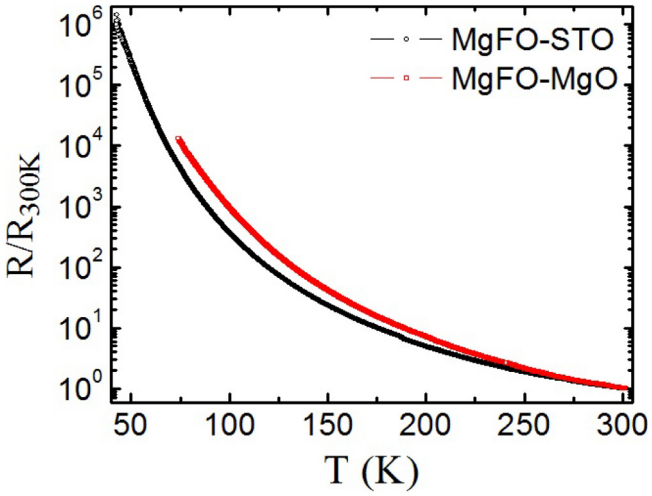

Fig. 6. Normalized resistance of samples MgFO-MgO and MgFO-STO as a function of temperature in the range 50 K–300 K.

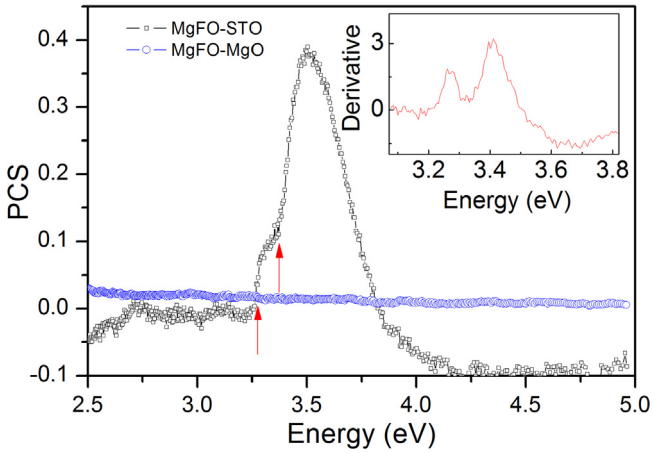

Fig. 8. Photoconductance as a function of the incident light energy for the sample MgFO-STO (black squares) and MgFO-MgO (blue circles) at room temperature. The direct and indirect band gap associated to STO substrate are indicated by arrows. Inset: PCS derivative.

Within the Mott VRH mechanism the parameter $\beta = 1/4$ and $1/3$ for three dimensional (3D) and 2D systems, respectively, for a constant density of states at Fermi level [34,35]. In our case, however, both samples show a dependence with $\beta = 1/2$, see Fig. 7(b). This β value corresponds to the case treated by Pollak, Knotek, Efros and Shklovskii [36–38] where in 2D and due to electron-electron interactions the resulting Coulomb gap derives in a linear in energy density of states at the Fermi level. From the fit of the curves $\ln(\rho/\rho_0)$ vs. $1/T^{0.5}$, we obtain $T^* \sim 27 \times 10^3$ K and 22×10^3 K for MgFO-MgO and MgFO-STO, respectively. This value is not yet reported for Mg ferrite system. However the obtained values are of the order of those reported for similar systems as BaTiO3 ($T^* = 44.8 \times 10^3$ K) [39].

The photoconductivity spectra (PCS) was measured in both samples at room temperature. *PCS* is defined as $PCS = [\sigma(h\nu) - \sigma_d]/\sigma_d$, $\sigma(h\nu)$ is the conductivity under illumination with photon energy $h\nu$ and σ_d is the conductivity in dark.

The PCS of MgFO-STO sample is shown in Fig. 8 (black squares). As can be seen PCS has an increase of 40 % when the sample is illuminated with near UV light. The photocurrent shows two clear onsets at 3.26 eV and 3.39 eV. The maxima in the derivative (see inset in Fig. 8) clearly identify the respective band gaps at 3.26 eV and 3.40 eV at room temperature. These photoconductivity edges matching with the indirect (~ 3.25 eV) and direct gap (3.40 eV) reported for $SrTiO_3$ [40]. These results confirm the fact that the measured resistance of the MgFO-STO sample should be treated as two conducting paths in parallel. Interestingly, above 3.50 eV the resistivity increases abruptly suggesting a strong recombination mechanism, which overwhelms the contribution to the conductivity of the direct gap photo carriers. This mechanism could be associated to surface/interface recombination centers. Our results suggest that the substrate plays an important role in the generation of photo carriers and the interfaces in the insulating MgFO thin film are sources of recombination centers. The thin film deposited on MgO does not exhibit significant photoconductivity at room temperature, as is shown in Fig. 8 (blue circles).

4. Conclusion

$MgFe_2O_4$ non-stoichiometric thin films on $SrTiO_3$ and MgO substrates were obtained by a FeO/MgO multilayer DC magnetron sputtering deposition. The morphology as well as the magnetic and transport properties show the effect of the substrate in this kind of systems. $MgFe_2O_4$ thin films have a magnetization at saturation higher than the reported for bulk $MgFe_2O_4$ at room temperature. This enhancement is due to the mixed oxidation state of iron that induce ferromagnetic coupling between Fe_B sites via double exchange interaction, in addition to the ferrimagnetism induced by the partial inversion that is usual in Mg ferrites. Both films show field hysteresis loops of rectangular shape at room temperature but the M_r/M_s relationship is higher in the MgFO-STO probably due to microscopic inhomogeneities and cell distortion (enlargment in the direction perpendicular to film plane), product of the higher mismatch between MgFO and STO. Whereas this characteristic remains at all temperatures in the MgFO-STO film, the

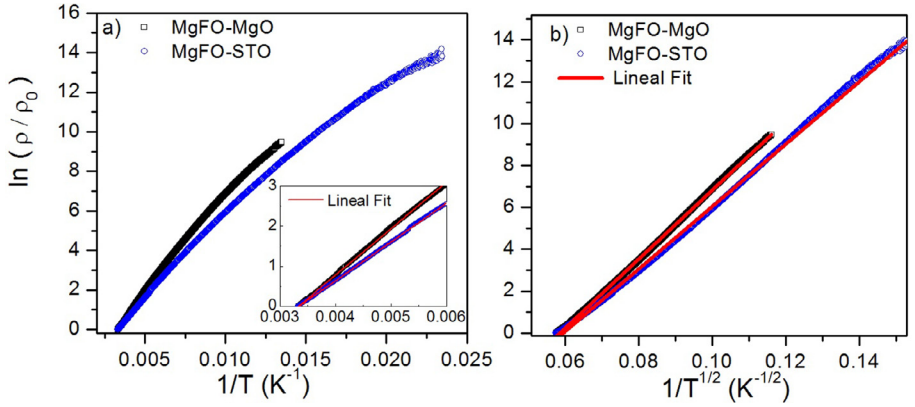

Fig. 7. (a) Normalized resistivity of MgFO-MgO and MgFO-STO samples as a function of temperature vs. inverse temperature. Inset: The same but in a smaller temperature range including linear fits to the data. (b) $\ln(\rho/\rho_0)$ vs. $1/T^{1/2}$ for both samples and the corresponding linear fits.

hysteresis of the film deposited on MgO and at $T < 300$ K, shows clear changes that indicate the presence of more than one magnetic component. Both samples show high resistivity at room temperature and semiconducting-like behaviour with different activation energies upon temperature range. The MgFO-STO sample presents an increase around 40% of the photoconductance in the near UV range at room temperature due to the indirect and direct band gaps of the $SrTiO_3$ substrate. The results strengthen this ferrite system as a candidate for optical and/or magneto-optical sensors and storage device applications.

Acknowledgement

This work was supported by the German Academic Exchange Service (DAAD) and the Ministry of Science, Technology and Productive Innovation of the Republic of Argentina, by means of the scientific project: "Experimental and theoretical Investigations of defect induced ferromagnetism at room temperature in Ferrites" (Project ID: 57052290 or DA13/02 MINCYT) and the collaborative Project SFB 762 from the DFG in Germany; Brazilian Synchrotron Light Laboratory-LNLS (proposals PGM-20160228 and XAFS2-20160122); CONICET (PIP 908 and PIP 585); ANPCyT, Argentina (PICT 2013–2616 and PICT 2016–3356) PICT- No. 2016–3356, PIP 585 and SNMAG facilities. The authors thank Dr. Israel Lorite and Dr. Yogesh Kumar for helping in the magnetic measurements performed at the Felix-Bloch Institute for Solid State Physics, University of Leipzig (Germany) and Dr. Benjamin Straube for helping in the transport measurements carried out at the Solid Physics Laboratory, National University of Tucumán (Argentina).

References

[1] I. Bakonyi, L. Pter, Electrodeposited multilayer films with giant magnetoresistance (GMR): progress and problems, Prog. Mater Sci. 55 (2010).
[2] M. van Zalk, J. Huijben, U. Zeitler, J.C. Maan, Wilfred Gerard van der Wiel, G. Rijnders, D.H. Blank, H. Hilgenkamp, A. Brinkman, M. Huijben, Magnetic effects at the interface between non-magnetic oxides, Nat. Mater. 6 (2007).
[3] H.Y. Ohtomo, A. Hwang, A high-mobility electron gas at the LaAlO3/SrTiO3 heterointerface, Nature 427 (2004).
[4] F. Trier, D.V. Christensen, F.M. Qu, N.H. Andersen, T. Kasama, W. Zhang, R. Giraud, J. Dufouleur, T.S. Jespersen, J.R. Sun, A. Smith, J. Nygrd, L. Lu, B. Bchner, B.G. Shen, S. Linderoth, Y.Z. Chen, N. Bovet, N. Pryds, A high-mobility two-dimensional electron gas at the spinel/perovskite interface of γ-Al2O3/SrTiO3, Nat. Commun. 4 (2013).
[5] Kebede K. Kefeni, Titus A.M. Msagati, Bhekie B. Mamba, Ferrite nanoparticles: synthesis, characterisation and applications in electronic device, Mater. Sci. Eng., B 215 (2017) 37–55.
[6] Al Lehyani Sha, Hassan Ra, Alharbi Aa, T. Alomayri, H. Alamri, Magnetic hyperthermia using cobalt ferrite nanoparticles: The influence of particle size, Int. J. Adv. Technol. 8 (4) (2017) 196.
[7] Marin Schwarz, Milo Veverka, Eva Michalkov, Vladimr Lalk, and Darina Veverkov, Utilisation of industrial waste for ferrite pigments production, Chemical Papers, 2012.
[8] C. Su, Environmental implications and applications of engineered nanoscale magnetite and its hybrid nanocomposites: s review of recent literature, J. Hazard Mater. 322 (Pt A) (2016) 48–84.
[9] K. Bagani, S. Majumder, A. Roychowdhury, S. Banerjee, V.R. Reddy, D. Das, S. Dey, S.K. Dey, S. Kumar, Overcoming inherent magnetic instability, preventing spin canting and magnetic coding in an assembly of ferrimagnetic nanoparticles, Appl. Phys. Lett. 105 (2014) 063110.
[10] R.N. Bhowmik, R. Ranganathanv, S. Sarkar, C. Bansal, R. Nagarajan, Magnetic enhancement of Co0.2Zn0.8Fe2O4 spinel oxide by mechanical milling, Phys. Rev. B 68 (2003) 134433.
[11] S. Majumder, S. Dey, K. Baganiand, S.K. Dey, S. Banerjeeb, S. Kumara, A comparative study on structural, optical and magnetic properties of Fe3O4 and Fe3O4@SiO2 core-shell microspheres along with assessment of their potentiality as electrochemical double layer capacitor, Dalton Trans. 44 (2015).
[12] S.K. Jana, S. Majumder, B. Satpati, S.K. Mishra, R.K. Srivastava, S. Banerjee, Enhancement of photoluminescence emission and anomalous photoconductivity properties of Fe3O4@SiO2 core-shell microsphere, RSC Adv. 5 (2015) 37729.
[13] S. Majumder, B. Saha, S. Deyb, R. Mondal, S. Kumar, S. Banerjee, A high sensitive non-enzymatic hydrogen peroxide and hydrazine electrochemical sensor based on 3d microsnowflakes architectures of α-Fe2O3, RSC Adv. 6 (2016) 59907.
[14] Y. Shimizu, H. Arai, T. Seiyama, Theoretical studies on the impedance-humidity characteristics of ceramic humidity sensors, Sens. Actuat. 7 (1985).
[15] G. Busca, E. Finocchio, V. Lorenzelli, M. Trombetta, S.A. Rossini, Ir study of alkene allylic activation on magnesium ferrite and alumina catalysts, J. Chem. Soc., Faraday Trans. (1996).
[16] S. Majumder, S. Kumar, S. Banerjee, Nanometric MgFe2O4: synthesis, characterization and its application towards supercapacitor and electrochemical uric acid sensor, AIP Conf. Proc. 1832 (2016).
[17] Muhammad Shahid, Jingling Liu, Zahid Ali, Muhammad Farooq Warsi, Photocatalytic degradation of methylene blue on magnetically separable MgFe2O4 under visible light irradiation, Mater. Chem. Phys. 139 (2013).
[18] Yue Pan, Ying Zhang, Xiaopei Wei, Congli Yuan, Jinling Yin, Dianxue Cao, Guiling Wang, MgFe2O4 nanoparticles as anode materials for lithium-ion batteries, Electrochim. Acta 109 (2013).
[19] Alex Dagg, Yang Hou, Fan Zuo, Pingyun Feng, A three-dimensional branched cobalt-doped α-Fe2O3 nanorod/MgFe2O4 heterojunction array as a flexible photoanode for efficient photoelectrochemical water oxidation, Angew. Chem. Int. 52 (2013).
[20] Seung Ho Han, Jeong Seog Kim, Ho Gi Kim, Chae Il Cheon, Kyoung Sun Kim, P. Muralidharan, Influence of oxygen partial pressure on the epitaxial MgFe2O4 thin films deposited on SrTiO3 (100) substrate, J. Alloy. Compd. 503 (2010).
[21] R.K. Gupta, F. Yakuphanoglu, Epitaxial growth of MgFe2O4 (111) thin films on sapphire (0001) substrate, Mater. Lett. 65 (2011).
[22] Cormac Coileáin, Askar Syrlybekov, Abbas Khalid, Anas Mouti, Mourad Abid, Hong-Zhou Zhang, Mohamed Abid, Igor V. Shvets, Han-Chun Wu, Ozhet Mauit, Magnetic and transport properties of epitaxial thin film MgFe2O4 grown on MgO (100) by molecular beam epitaxy, Sci. Rep. 4 (2015).
[23] P. Mendoza Zélis, G.A. Pasquevich, K.L. Salcedo Rodríguez, F.H. Sánchez, C.E. Rodríguez Torres, Surface magnetic contribution in zinc ferrite thin films studied by element- and site-specific xmcd hysteresis-loops, J. Magn. Magn. Mater. 419 (2016).
[24] Karen Lizeth ,Salcedo Rodríguez, PhD thesis.
[25] Al Mamun, Shireen Akhter, Md. Tanvir Hasan, Deba Prasad Paul, Kamanio Chattopadhayay, Sheikh Manjura Hoque, M. Abdul Hakim, Study of the bulk magnetic and electrical properties of MgFe2O4 synthesized by chemical method, Mater. Sci. Appl. 2 (2011).
[26] A. Poddar, C. Mazumdar, S. Banerjee, V.R. Reddy, B. Ghosh, S. Kumar, A. Gupta, Spin glasslike behavior and magnetic enhancement in nanosized NiZn ferrite system, J. Appl. Phys. 108 (2010) 034307.
[27] J. Cheng, V.K. Lazarov, G.E. Sterbinsky, B.W. Wessels, Synthesis, structural and magnetic properties of epitaxial MgFe2O4 thin films by molecular beam epitaxy, J. Vacuum Sci. Tech. B 27 (2009).
[28] Han-Chun Wu, Ozhet Mauit, Cormac Coilein, Askar Syrlybekov, Abbas Khalid, Anas Mouti, Mourad Abid, Hong-Zhou Zhang, Mohamed Abid, Igor V. Shvets, Magnetic and transport properties of epitaxial thin film MgFe2O4 grown on MgO (100) by molecular beam epitaxy, Sci. Rep. 4 (2014).
[29] M.A. Zinovik, E.V. Zinovik, Ferrites with rectangular and square hysteresis loops, Powder Metall. Met. Ceram. 44 (2005).
[30] S. Brice-Profeta, M.-A. Arrio, E. Tronc, N.MenguyandI. Letard, C. Cartier dit Moulin, M. Nogus, C. Chanéac, J.-P. Jolivet, Ph. Sainctavit, Magnetic order in α-Fe2O3 nanoparticles: a xmcd study, J. Magn. Magn. Mater. 288 (2005).
[31] C.E. Rodríguez Torres, G.A. Pasquevich, P. Mendoza Zélis, F. Golmar, S.P. Heluani, Sanjeev K. Nayak, Waheed A. Adeagbo, Wolfram Hergert, Martin Hoffmann, Arthur Ernst, P. Esquinazi, S.J. Stewart, Oxygen-vacancy- induced local ferromagnetismas a driving mechanism in enhancing the magnetic response of ferrites, Phys. Rev. B 89 (2014).
[32] J. Smit, H.P.J. Wijn, Ferrites, Philips Glocilampenfabrieken, Eindhoven, 1959.
[33] A. Spinelli, M.A. Torija, C. Liu, C. Jan, C. Leighton, Electronic transport in doped SrTiO3: conduction mechanisms and potential applications, Phys. Rev. B S1 (2010).
[34] N. Mott, E. Davis, Electronic Processes in Non-Crystalline Materials.
[35] N.F. Mott, Conduction in glasses containing transition metal ions, J. Non-Crystalline Solids 1 (1968).
[36] M. Pollak, Effect of carrier-carrier interactions on some transport properties in disordered semiconductors, Discuss. Faraday Soc. 50 (13) (1970).
[37] M.L. Knotek, M. Pollak, Correlation effects in hopping conduction: hopping as a multi-electron transition, J. Non-Cryst. Solids 505 (1972).
[38] A.L. Efros, B.I. Shklovskii, Coulomb gap and low temperature conductivity of disordered systems, J. Phys. C8 (1975) L49.
[39] Hyuk Su Han, Calvin Davis III, Juan C. Nino, Variable range hopping conductionin batio3 ceramics exhibiting colossal permittivity, J. Phys. Chem. C 17 (2014).
[40] G. Bridoux, M. Villafuerte, M. Ferreyra, N. Bachi, C.A. Figueroa, S.P. Heluani, Light-induced metal-insulator transition in SrTiO3 by photoresistance spectroscopy, Phys. Rev. B 92 (2015).